Electron spin resonance probing of fundamental point defects in nanometer-sized silica particles

A. Stesmans, K. Clémer, and V. V. Afanas'ev
Department of Physics and Astronomy, University of Leuven, 3001 Leuven, Belgium
(Received 6 October 2004; revised manuscript received 15 April 2005; published 31 October 2005)

Point defects in fumed ~7-nm-sized silica nanoparticles have been studied by *K*- and *Q*-band electron spin resonance (ESR) following 10-eV irradiation used to photodissociate H from passivated defects. Various types of ESR-active point defects are revealed, including the familiar E' center (generic entity $\cdot Si{\equiv}O_3$), EX, the peroxy radical (POR), the methyl radical, and an unknown closely axially symmetric center ($g_{\parallel}=2.0041$, $g_{\perp}=2.0027$). The possible atomic nature of the latter is addressed. The E' defects, occurring in a maximum density of $\sim 1\times 10^{-3}$ per nanoparticle, are monitored as a function of thermal treatment in vacuum in the range 850–1115 °C in order to assess specific physicochemical structural aspects of the particles. Experimental evidence is presented for the presence of two different systems of E' centers. The specific ESR parameters of the E' centers of one bath are found to be very similar to those of the E'_{γ} center in bulk fused silica, while the second bath exhibits a different zero crossing g value and line shape, attributed to variations in local structure. It is inferred that the latter E' system pertains to the outer SiO_2 layers, exposing a structural nature different from bulk glassy SiO_2. Besides PORs, large numbers of other oxygen-hole type defects appear to be present also. The exhaustive number of all oxygen-hole centers, including the PORs, is determined at ~0.07 defects/nanoparticle, making this kind of defect highly unlikely as playing a substantial role in narrowing of the optical bandgap, in contrast with previous suggestion.

DOI: 10.1103/PhysRevB.72.155335 PACS number(s): 61.46.+w, 61.72.Ji, 68.35.Dv, 76.30.Mi

I. INTRODUCTION

Fumed silica's have been commercially produced since the 1940s. The nanoparticles found numerous applications.[1,2] For instance, they can be found as fillers in toothpaste and car tires, as starting material for optical fibers, and may serve as a general gel former.[1] The incessant tendency however of today's industry towards miniaturization—the nanotechnology era—has renewed interest in these nm-sized silica particles for their diverse range of potential applications ranging from electronics, optical nanodevices to catalysis, chromatography, and biosensors.[2,3] It is therefore important to have a good understanding of the properties of nanoparticles *vis-à-vis* those of the macroscopic counterparts as well from a fundamental as an applied point of view. Little is known yet about the exact structure of fumed silica: However, as perceived, the nanoparticles are in the amorphous phase, interpreted as being caused by the extremely fast cooling of the pyrogene silica aggregates formed at 1400–1800 °C. They have been intensively studied theoretically[4–8] as well as by a range of sensitive experimental techniques,[9–17] such as positron annihilation,[10] x-ray diffraction,[11] and the key photon-solid interaction probes including optical[14] and Fourier transform infrared (FTIR) absorption,[9,11,17] Raman spectroscopy,[11] nuclear magnetic resonance (NMR),[15] and electron spin resonance (ESR).[10,16]

These studies on silica nanoparticles indicate that their structure, and associated optical and electronic properties, distinctly differ from those of the bulk SiO_2 glasses.[11,14,17] Assumedly, this is due to the higher concentration of occurring structural (inherent) defects, without doubt in part related to the exorbitant surface area/volume aspect ratio. An FTIR study of dissociative chemisorption[9] on dehydroxylated fumed silica indeed showed the presence of highly reactive defect sites. The faster hydrolization of these defects, a factor 10^5 to 5×10^6 higher as compared to fused silica, indicates that the reactivity of the Si-O bonds is promoted by bond strain. An extensive NMR research[15] points out that both mutually hydrogen-bonded and isolated silanols (Si-OH groups) are present at the surface of fumed silica, but only the isolated ones remain after heating at a temperature $T>350$ °C. This work also concluded that the high temperature production of the nanoparticles leads to a wider range of variation of Si-O-Si bond angles. In other works, the difference in photoluminescence (PL) properties[12,13] of the silica nanoparticles as compared to bulk fused silica was assigned to the presence of a large concentration of surface nonbridging oxygen-associated hole centers (NBOHC's). It is stated that such defects are introduced during particle formation and further increase in density after heat treatment of the silica powder in air at anneal temperatures (T_{an}) in excess of 600 °C. The researchers suggested that these defects dominate the PL spectrum in samples heat treated at $T_{an}=900$ °C. Later on, this picture was retained when the nonexponential absorption of light[14] was attributed to a drastic change in band structure ensuing from a high concentration of such structural defects. However, ESR, the tool eponymous for their occurrence, has so far provided no evidence for the named point defects.

Recent work[11] has concluded a different, more flexible network structure consisting of small-membered rings for silica nanospheres as compared to that of bulk silica glass. According to the FT-Raman spectra these small-membered rings still survive after heating up to 1100 °C, but at 1200 °C bulklike silica is formed. The onset temperature for sintering, however, is 800 °C, as evidenced by a study of the specific surface area. Previous molecular dynamics (MD) computer simulations concluded a shell-like structure of the nanoparticles.[4,5] The surface has a different density and

structure as compared to the interior of the cluster, which is suggested to be structurally equivalent to bulk silica. The latter though was countered by Uchino *et al.*, who concluded from their infrared measurements that the structure of the interior of the nanoparticles cannot be equivalent to that of macroscopic SiO_2.[11]

It has been demonstrated that inherent structural defects, as studied by the electron spin resonance technique, may serve as atomic sized probes of utmost sensitivity to structural aspects of their local environment [see, e.g., Refs. 18–20]. So, their characterization and identification may appear a key means to assess the structural nature of the nanoparticles and to reveal possible differences as compared to the bulk silica counterpart. Though being a tool with atomic level physico-chemical sensitivity, very little research has so far been carried out using ESR: Some ESR work has been done on fumed silica in the as-grown state[16] as well as after uv irradiation[10] with photons (~5 eV) obtained from a low pressure Hg lamp. However, in both cases no ESR signals originating from the silica nanoparticles could be observed, likely explaining the faded interest over the years in applying ESR to this field of research. In view of the particular preparation method of fumed silica particles (see below), this ESR failure is possibly due to the fact that occurring (inherent) point defects may be left passivated by bonding to hydrogen (H) in the as-prepared state, thus rendering them ESR inactive. Such phenomenon is well known for Si dangling bond type defects such as the P_b ($Si_3{\equiv}Si$)[19,21,22] and E' defects[23] in thermal Si/SiO_2. In this context, it is pertinent to note that the applied uv irradiation may energetically appear just not sufficiently efficient to reactivate defects to a detectable amount. On this matter, vuv excitation proves to be much more appropriate.[24,25] Combining such photon excitation (~10 eV) with ESR analysis, the current work reports on the first direct ESR observation and identification of fundamental point defects in fumed silica nanoparticles. The occurring ESR resonances are monitored as a function of postformation heating and treatment (aging, vuv excitation) with a view to asses structural aspects of the nanoparticles.

II. EXPERIMENTAL DETAILS

A. Samples

The samples studied were taken from high-purity pyrogene fumed silica powder of 7 nm average particle size and 380 ± 40 m^2/g surface area, with a "bulk" density of 36.8 g/dm^3 and low metallic impurity content.[26] The structure of the material is amorphous. During particle formation and subsequent cooling down, interparticle collisions and subsequent fusion results in the formation of chainlike aggregates from 10 to 30 units, or, put differently, from ~0.1 to 0.2 μm in length. Since fumed silica is fabricated by burning silicon tetrachloride in an oxygen-hydrogen flame at ~1800 °C, nominally there should be no carbon present.

Separate sets of samples (fresh ones for each thermal step) were subjected to postmanufacturing baking in vacuum (base pressure $<4\times10^{-6}$ Torr) for ~1 h at desired temperatures (T_{an}) in the range 850–1115 °C.

B. Electron spin resonance spectroscopy

Conventional cw absorption-derivative (dP_μ/dB) *K* (~20.3 GHz) and *Q*-band (~33 GHz) ESR measurements[19] were performed in the range 4.2–300 K, both spectrometers being equipped with a TE_{011} cavity. The modulation amplitude B_m of the applied magnetic field **B** and incident microwave power P_μ were restricted to levels not causing (noticeable) signal distortion. The latter is very pertinent with respect to inferring reliable ESR parameters of highly saturable point defects, such as, e.g., the E' center in bulk SiO_2. To avoid saturation effects, most *Q* band measurements were carried out at ~100 K as reducing P_μ (required along with cooling lower) is limited by the performance of the automatic frequency control (AFC). A comounted calibrated Si:P marker sample [spin $S=\frac{1}{2}$; $g(4.2\ \mathrm{K})=1.99869$] was used for *g* factor and defect (spin) density calibration. The latter was attained by comparing the intensities obtained through orthodox double numerical integration of the detected derivative absorption spectra of the point defect in question in the studied sample and the marker, both recorded in one trace. In the case of broad powder pattern spectra, e.g., the NBOHC signal, this procedure was aided by computer-assisted simulation of the observed spectra. Signal averaging was applied (typically 10–30 scans for *K*-band and 100–300 scans for *Q*-band measurements) to enhance and optimize signals. Typically, an ESR sample comprised ~3–4 mg of fumed powder, with physically the same samples being used for both *K* and *Q*-band ESR observations.

From previous investigations it may be anticipated that in the as-reacted state fumed silica, the particular pyrolytic fabrication technique applied (oxy-hydrogen flame) may result in passivation of dangling-bond type point defects by hydrogen (pictured as ≡SiH, ≡Si-OH formation), thus leaving possibly occurring inherent systems of defects in the diamagnetic state and hence disabling ESR detection. More specifically, for defects such as the E'_γ centers, the occurring (passivated) precursor site is pictured as the $O_3{\equiv}Si\text{-}H$ entity at the site of an O vacancy,[27,28] while, similarly, for the NBOHC, $O_3{\equiv}Si\text{-}OH$ (hydroxyl incorporation into the silica matrix) is pictured as an obvious site.[27] So, after initial ESR tests, to maximally reveal defects, samples (both in the as-grown state and after additional heat treatment) were subjected at room temperature (RT) to prolonged irradiation by vuv (10 eV) photons (flux $\sim10^{15}$ cm^{-2} s^{-1}) obtained from a Kr-resonant discharge lamp sealed with a MgF_2 window to photodissociate H from passivated defects, or put differently, to radiolyze defect-H bonds. Possibly, the treatment may additionally unveil strained or weak bondings (bond rupture) and diamagnetic precursor sites.[24]

Here, it may be appropriate to shortly digress on this. One known mechanism one may envision concerns defects created radiolytically via nonradiative recombination of a self-trapped exciton.[23,27] In principle, such radiolytic damage can be induced by virtually any type of radiation with kinetic energy per impinging particle ⩾9 eV (i.e., the band gap of SiO_2), enabling over band gap excitation. In an elucidating ESR work,[29] the bearing of this notion is underpinned prominently through evidencing the importance of the two-photon processes in photogeneration of E' centers in silica by sub-

TABLE I. Overview of typical densities of the observed defects as a function of the anneal temperature T_{an} and vuv treatment. Quoted values are in units of 10^{14} g^{-1}. To convert the densities to units of 10^{14} cm^{-3}, multiply by 2.3. Entries left blank means the corresponding defect could not be detected or the signal appeared too weak for reliable discrimination.

Sample condition	[E']	[LU2]	[OHC]	[EX]	[CH_3]
As-grown					
As-grown+vuv[a]	2.2±0.5		31±3		0.08±0.01
T_{an}=850 °C		0.52±0.05			
T_{an}=850 °C+vuv[a]	2.4±0.5				0.47±0.05
T_{an}=850 °C+vuv[b]	1.0±0.5				
T_{an}=960 °C		60±6		2±1	
T_{an}=960 °C+vuv[a]	1.5±0.5	7.3±0.8		2±1	0.14±0.02
T_{an}=1005 °C				7±0.5	
T_{an}=1005 °C+vuv[a]	3±1			1.5±0.2	0.07±0.01
T_{an}=1115 °C				49±5	
T_{an}=1115 °C+vuv[a]	3.5±1			21±3	

[a]The densities given here are obtained from samples subjected to ~1 h vuv irradiation.
[b]Several days after vuv irradiation, the samples being left in room ambient.

bandgap photons. For subbandgap (photon) excitation, one specifically suggested mechanism is pair generation of E' and NBOHC defects through photo induced breaking (photon energy $\geqslant$7.9 eV) of strained Si-O bonds in highly strained 3-membered SiO rings in silica.[30–32] However, the relative contribution of these strained network bond breaking processes to the total of the vuv-stimulated production process of ESR active defects is not considered dominant. In a related work, a value of ~30 eV was suggested for E' creation through breaking of a bond in the SiO_2 network at a previously completely bonded site.[33] Creation appears a far less genuine process than defect activation. But even in the case that a (limited) part of ESR-active defects would be *created* this way, it should also add to the ultimate goal. That is, acquiring atomic scale information about the SiO_2 particles network, as these sites of defect creation, i.e., strained and/or weak bonding sites, constitute in embryo also imperfections in the *a*-SiO_2 matrix, albeit not nonstoichiometry defects right away.

Hydrogenic species ($H, OH, H_2O, \ldots$) may of course also be removed—dehydrogenation—through baking at high T in H-deficient ambient. For example, it is known that efficient dehydroxylation is attained by heating[11] in vacuum at T ~900 °C. However, besides the fact that this procedure cannot be applied for studying the influence of annealing in the T_{an} range below the required high anneal temperature for H removal, it will, in the T range covered, also fail on a different account for some particular point defects, like, e.g., the E'-type center, which is known to exhibit an excessively high activation energy for dissociation[34–36] ($E_a \sim 4.5$ eV). Moreover, baking at high T may affect irreversibly the as-grown network structure of the nanoparticles, which initial state is also an envisioned target of the current study.

Early on in this work aging effects have been observed to occur in room ambient for at least one defect (*vide infra*). So ESR measurements were first performed immediately upon vuv irradiation and subsequently repeated after the samples were left in room ambient for desired times (one day to weeks). This enabled us to study the characteristics of defect modification in room ambient.

III. RESULTS AND ANALYSIS

As anticipated, no ESR signal could be observed in the as-fabricated silica particles. This is ascribed, at least in part, to defect inactivation by hydrogen due to the abundance of H_2 during the flame growth. But that situation changes drastically upon vuv irradiation or after annealing at high temperature. Several signals are observed, their proper spectroscopic isolation, though, being strongly hampered by signal overlap and entanglement. As a result, while at least 5 types of signals could be assigned and analyzed, several interesting resonant responses (mostly of low intensity) remain as yet unidentified. Table I gives an overview of observed defect densities as a function of post-manufacture heating and vuv treatment. These defects will now be addressed separately.

A. E' type center

1. Observations

After vuv irradiation, the SiO_2-specific E' type center (generic entity $O_3{\equiv}Si\cdot$) is clearly detected in the as-grown sample, as displayed in Fig. 1, as well as in the samples subjected to postmanufacture baking. A characteristic central-line two-peak powder pattern signal is observed much similar (e.g., regarding width, overall shape) to that of the common E'_γ variant[37,38] (modeled as the $O_3{\equiv}Si\cdot\ldots{}^{+}Si{\equiv}O_3$ defect) in bulk silica, characterized by[39] the principal g matrix values g_1=2.0018, g_2=2.0006, and g_3=2.0003. In the *K* band ESR spectroscopy a zero crossing g value of g_c=2.00058±0.00005 is typically observed[40] in thermally grown SiO_2 on Si. Detailed computer simulations of the presently observed spectra show slight, but convincing, variations in ESR parameters depending on the applied

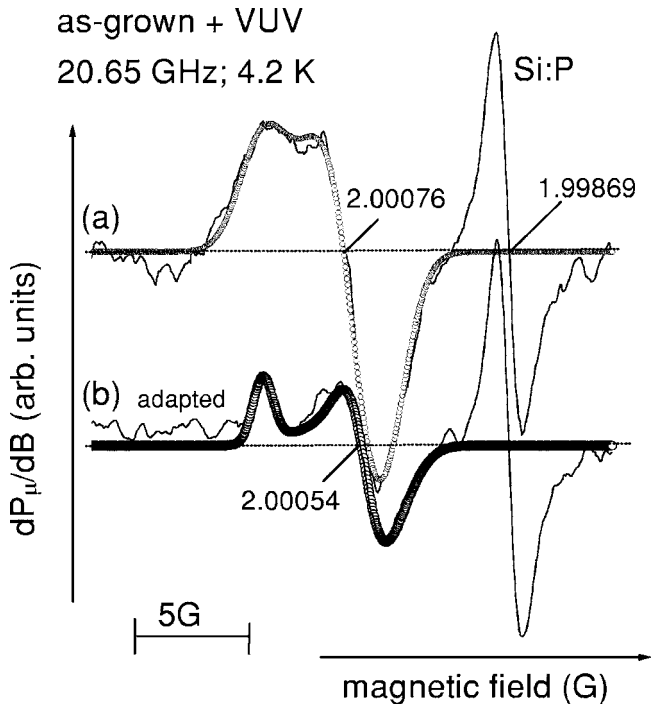

FIG. 1. Powder pattern K-band ESR spectra ($P_\mu \sim 0.05-0.2$ nW; $B_m=0.35-0.5$ G) of E' centers measured at 4.2 K (a) immediate upon vuv irradiation and (b) several days later, the sample being left in room ambient. Symbols (circles) represent spectra simulations employing Gaussian broadening functions. The used g values and corresponding peak-to-peak derivative linewidths are (a) $g_1=2.00174$; 2.1 G, $g_2=2.00070$; 2.3 G, $g_3=2.00030$; 2.2 G; (b) $g_1=2.00174$; 0.9 G, $g_2=2.00048$; 1.4 G, $g_3=2.00017$; 2.1 G.

anneal temperature, elapsed time period between vuv irradiation and ESR measurement as the sample was kept in room ambient, and the sample temperature during the measurements.

In the as-grown sample, measured immediately after vuv irradiation, the observed zero-crossing g value $g_c=2.00076\pm0.00005$ is slightly, yet well outside experimental error, larger than the one observed for irradiated thermally grown SiO_2 on Si or fused silica, i.e., $g_c=2.00058\pm0.00005$.[38,40] Additional heat treatment, however, affects the E' signal distinctly. Upon annealing at increasingly higher temperatures in the range $T_{an}>850$ °C, the zero-crossing g value gradually decreases for $T_{an}\rightarrow 1115$ °C towards the value typically measured for E'_γ in bulk silica's. There is one more remarkable observation: Pertinently, when, after vuv irradiation, leaving the samples for substantial time (~days) in room ambient—henceforth, referred to as the *adapted state*—the zero-crossing g value has shifted to about the same value (towards $g_c=2.00054\pm0.00005$) for all the samples regardless of their heat treatment. These trends are exposed in Fig. 2, where g_c measured immediately upon vuv irradiation and after subsequent stay of the samples for days in room ambient, is plotted against T_{an}.

A second important ESR parameter is the displayed powder pattern line shape. A likely pertinent observation is that

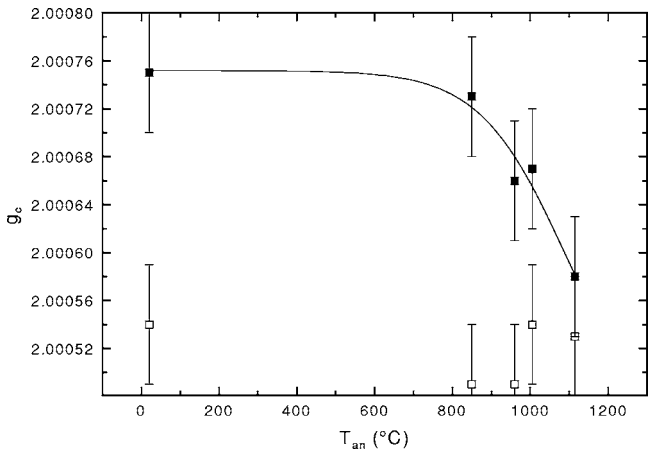

FIG. 2. Zero-crossing g value of the measured E' signal (K-band; 4.2 K) as a function of the heating temperature. Closed symbols: measured immediate upon vuv irradiation. Open symbols: several days later, the samples being left in room ambient.

the shift in g_c over time in room ambient is accompanied by an attendant variation in the displayed powder pattern line shape. As illustrated in Fig. 1(b), this implies, as general trend, evolution from a more blurred, broadened shape to a sharper, well expressed typical "two-peak" powder pattern pertaining to a nearly axially symmetric g matrix. A similar trend is observed as the measurements are carried out at different temperatures: The lower the sample temperature, the more blurred and broadened the powder pattern becomes, as illustrated in Fig. 3. At the same time a small variation in g_c is observed. Careful analysis leads to the conclusion that the latter variation in zero crossing g value is purely a conse-

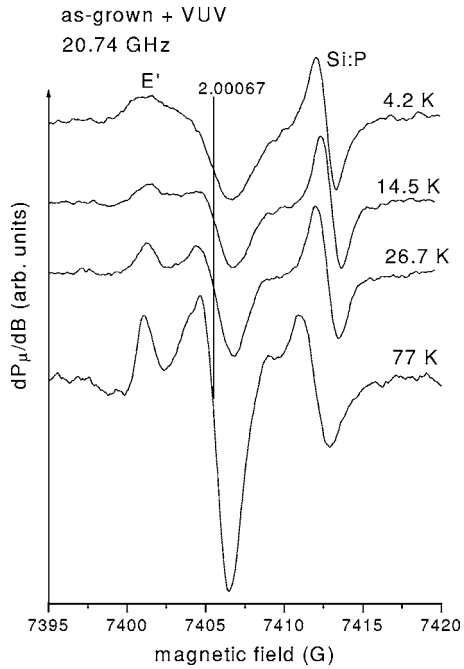

FIG. 3. Powder pattern K-band ($P_\mu \sim 2.5$ nW; $B_m \sim 0.6$ G) ESR spectra of the E' signal measured at different temperatures in the as-grown sample immediate upon vuv irradiation. It should be noted that, as known, g(Si:P) is temperature dependent.

quence of the attendant strong change in the line shape and has little to do with the g_c shifts mentioned before. As will be outlined later (Sec. III A 2), it is attributed to T-dependent surface strain adaptation.

A third ESR parameter able to provide important information is the defect (E') density. Immediately upon prolonged (days-week) vuv activation of the as grown particles, the maximum density that could be attained was determined as $(2.4\pm0.5)\times10^{15}$ g^{-1}, corresponding to about 1×10^{-3} defects/nanoparticle. It should be added though that this number may not represent the maximum number of E' type centers inherent to the fumed nanoparticles, as the vuv treatment may not have exhaustively activated all defect sites present due to the small penetration depth ($\sim$10 nm) of the vuv photons in SiO_2 in combination with the powder nature of the sample (geometric shadowing). However, the number may be close, given the prolonged irradiation treatment with regular intermittent stirring of the fumed powder. In support, doubling the irradiation time, indeed, did not increase any further the number of defects detected.

At this junction, it may be instructive to compare the observed E' densities with values encountered in other macroscopic silica (silica glass). Obviously, such comparison should be carried through most relevantly for defects produced by similar vuv treatment. A first most representative benchmark here may appear dry thermal SiO_2 grown on c-Si substrates, ubiquitously used in semiconductor integrated circuit (IC) technology and known to be of superb electrical quality, viz., in terms of point defect-related charge trapping centers. Remarkably, it is found here that the measured E' density is about 100 times smaller[41] than the densities typically observed[40] ($\sim1.4\times10^{17}$ g^{-1}) in thin ($\sim$4.1–6.5 nm thick) thermally grown dry SiO_2 on Si, indicating that the fumed silica is of superb quality in terms of malignant oxygen vacancies, that is, close to perfect SiO_2 stiochiometry or O-enriched. Further, it may be appropriate to add that the E'-type signal so far reported for thermal SiO_2 seems to be similar to the familiar E'_γ signal found in thicker layers. However, no detailed study appears available yet, without doubt partially because of limited ESR sensitivity. Second, in support of the nanoparticle quality, Tsai *et al.*[29] reported the photogeneration of E'_γ centers reaching densities $\geqslant10^{17}$ g^{-1} in high purity fused silica subjected to intense (40 mJ/cm^2 pulses; ArF laser) 6.4 eV photon irradiation. The E' production efficiency was found to increase with higher OH content, the E'_γ density, however, staying well below [OH].

A last but perhaps highly pertinent observation is that the observed shift in g_c over time as the sample is left in room ambient is accompanied by a striking *reduction in the E' signal intensity*. In the adapted state, the signal has reduced, in average, by a factor of $\sim2\pm0.5$.

Information on the hyperfine (hf) interaction is well known to be a key point in atomic identification of point defects. Several attempts were made to resolve some associated (^{29}Si) hf structure, however, so far without success, which is attributed to the low density of occurring defects and strong signal overlap.

2. Interpretation

For purposes of assessing possible specific structural characteristics pertaining to the a-SiO_2 network of the studied nm-sized silica particles, it may then appear interesting to analyze what the revealed distinct attributes of the observed E' signal may tell us about the center's local environment within the a-SiO_2 matrix they are imbedded in. But before initiating, as several distinct species of E' centers have been delineated over the years in glassy SiO_2, a basic quest concerns what particular type(s) of E' center we are actually dealing with in these fumed silica particles. Here, key information concerns the ESR observations on the particles in *the adapted state* or after postmanufacture heating at $T_{an}\geqslant1100$ °C, exposing the data to converge to a common signal, and there is little doubt that this concerns the familiar E'_γ variant: This conclusion is based on the observed g values (g matrix, g_c) and the exhibited (nearly axially symmetric) powder pattern line shape as supported by detailed computer simulations of the observed signals.[37,38,42]

More evidence for this conclusion is adduced by Table II where representative g value data are assembled for the relevant most prominent E'-type centers reported in the literature together with current E' (E'_{nano}) results. From this comparison also, it follows that the SiO_2 nanoparticles E' signal does not concern the axially symmetric E'_β (Ref. 27) and E'_s (Refs. 43,44) variant nor the extreme (regarding g matrix) orthorhombic $E'_{\alpha1}$ type.[27] One may remark, however, that the comparison of g matrix elements usually reported in the literature situates in the last significant digit, i.e., 10^{-4} (see, e.g., Ref. 39). Generally, without having taken special measures (e.g., usage of accurate absolute g marker samples or ingenious high accuracy methods for *in situ* measurement of the at-the-sample magnetic field), most g value specifications do not extend beyond the fourth decimal digit (corresponding to an absolute **B** field determination accuracy of $\sim$0.16 G and $\sim$0.36 G for X and K band, respectively). So, over the many g data in the literature, one encounters (slight) variations in the values reported for identical defects, urging some caution when intending to carry out comparisons—in particular, when looking for small systematic variations. To settle this, the only way out appears to first establish internal consistency. Thus, for normalization (calibration) purposes we have additionally calibrated within our ESR approach based on the usage of a single high accuracy g marker, the "standard" most widely studied E'_γ center produced in synthetic fused silica suprasil I by 1 MGy ^{60}Co γ irradiation. These g matrix element results, consistent within an absolute accuracy of 2×10^{-6} between K and Q-band experiments, are included in Table II as well. Finally, in terms of g data, Table II also puts in better perspective the observed difference between the E' systems in fumed SiO_2 particles in the adapted and non-adapted state.

As the key point of focus, what then causes the notable variations in E' features—that is, shift in g_c with attendant variation in powder pattern shape—for the other non-adapted sample states, i.e., in the as-grown state or after heating in the $T_{an}<1100$ °C range, both just after vuv irradiation? Obviously, there may be various reasons.

One pertinent experimental observation is that the shift in g_c during post vuv excitation decay or after heating at $T_{an}>850$ °C appears persistently accompanied by a decrease in overall E' intensity, which would indicate that part of the ESR active centers drop out. The further interpretation could

TABLE II. Comparison of experimental principal-axis g matrix values of generic E' centers in irradiated high purity silica and synthetic quartz crystal. The general accuracy on g is ±0.0001 unless marked differently. For clarity, the shorthand notation such as, e.g., 2.00176(5) means 2.00176±0.00005.

E' type	g_1	g_2	g_3	Ref.	Sample	Damage
$E'_{\alpha 1}$	2.0018	2.0013	1.9998	27[a]	synthetic fused silica	100 keV x rays; 77 K
E'_{β}	2.0018	2.0004	2.0004	27[a]	synthetic fused silica	100 keV x rays; 77 K
E'_{s}	2.0018	2.0003	2.0003	43	natural and synthetic quartz	UHV crushing; 300 K
E'_{γ}	2.0018	2.0006	2.0003	27[a]	synthetic fused silica	100 keV x rays; 77 K
	2.00176(5)	2.00049(5)	2.00029(5)	42[b]	synthetic quartz crystal	Neutrons
	2.00175(4)	2.00056(4)	2.00030(4)	This work[c] Fused silica	suprasil I synthetic silica[d]	1 MGy ^{60}Co γ rays; 300 K
E'_{nano}	2.00174(4)	2.00070(4)	2.00030(4)	This work[c] 7 nm particles unadapted	fumed 7 nm particles *unadapted*	10 eV photons;[e] 300 K
	2.00174(4)	2.00048(4)	2.00020(4)	This work[c] 7 nm particles adapted	fumed 7 nm particles *adapted*	10 eV photons;[e] 300 K

[a]The $g_1=2.00176$ was taken from the literature.
[b]g values determined relative to a powdered diphenyl picryl hydrazyl marker with assumed g value of 2.0036.
[c]g values determined relative to Si:P g marker [$g(4.2\ \text{K})=1.99869\pm0.00002$].
[d]Obtained from Heraeus (Germany) containing [OH]$\sim$1200 ppm (by weight); [H_2O]$\leqslant$600 ppm, and total metal content $<$1 ppm.
[e]Obtained from a Kr-resonant discharge lamp; flux $\sim 10^{15}$ cm^{-2} s^{-1}.

then take two points of view: A first one could start from the occurrence of only one E'_{γ} system, yet characterized by a profound distribution in ESR broadening parameters. The applied vuv excitation would efficiently ESR activate centers all over the distribution. Then, during the subsequent stay in room ambient (*adaptation* period), part of the E' centers, perhaps due to environmental influence, would become gradually ESR inactivated (passivated), predominantly starting with those centers pertaining to the (extreme) tails of the ESR parameter distributions. Thus, with progressing inactivation, the more standard E'_{γ} signal would naturally surface, characteristic of macroscopic glassy SiO_2 with more standard spreads in relevant ESR broadening parameters.

In a second scenario, the more distorted part of the E'_{γ} centers, making up the extended tails of the g distributions, could be rather seen as stemming from a separate, second E' system. In an idealized scheme, one could picture the first, more bulk a-SiO_2-like E'_{γ} system as constituting the centers located more in the center ("bulk") of the nm-sized silica particles; The second system would comprise the defects pertaining to the structurally more distorted (strained) surface and near surface layers—the *surface E′ system*—more apt to environmental chemical and physical interaction (adsorption) impact. (About 10% of the molecules belongs to the surface area of a 7-nm SiO_2 particle.) Thus the E' signal might then rather be considered as the superposition of (at least) two overlapping signals originating from two separate E'_{γ} defect systems. The first bath is dominant in the spectra of the particles in the adapted state or after post-manufacture heating at $T_{\text{an}} \geqslant 1100$ °C leading to the observation of signals with very similar principal g values and g value distributions as the E' systems observed in bulk silica. The surface E' system is dominant in the spectra of the as grown sample immediate after vuv irradiation giving rise to a shift in g_c and an overall more broadened spectrum. For the remainder, the decay (adaptation) scenario upon vuv activation would be similar to the previous view: The second surface E' system would be *gradually* inactivated with increasing dwell time in room ambient, ultimately leaving only the first E'_{γ} bath. (The time delay may result from the altering accessibility by ambient species of E' centers located deeper in near surface layers). Interestingly, such a decrease in E' signal intensity has been observed before in the study of quartz crushed in vacuum.[43] There, an E'_{γ}-like (but not identical) signal was observed which could be readily modified by interaction with active gases, such as CO_2 and air. It is taken as evidence for the occurrence of surface dangling Si orbitals, i.e., the surface E' center,[38,41,43,44] termed E'_s, assigned to the hemicenter structure ($O_3{\equiv}Si\cdot$) at the grain surface. A similar sensitivity of Si dangling hybrids (D center) to the ambient has long ago been demonstrated at the surface of Si in cracks penetrating from the surface.[45]

The surface E' systems observed in crushed silica particles and thin deposited a-SiO_2 film on Si are characterized by a closely E'_{γ}-like g matrix, yet with a slightly *smaller* g_c value ($\sim$2.0003),[38,43] which would conflict with the current observations. However, here it should be remarked that in spectroscopical terms, as outlined above, the measured upward shift in g_c may well result from a substantial distribution in ESR parameters. Such spreads are well known to arise from amorphous-state disorder,[39,46,47] reflecting structural and strain induced site-to-site variations in Si-O-Si bond angles. Besides, it should be added that currently we deal with surfaces of nm-sized particles, which may exhibit a

distinctly different dimension of distortion as compared to bulklike grains and films. Thus, rather than counter, the current first report of such E' system from the outer layers of nm-sized silica particles might just instead be taken as evidence exposing this.

The overall broadened spectra observed for the as-grown state sample immediately after vuv irradiation and the strong temperature dependence of the linewidth may also be understood as the result of the presence of a surface E' system. It seems reasonable to accept that the outer layers of the nanoparticles have a somewhat more distorted, more strained structure as compared to the inner core of the particles. Molecular dynamics computer simulations did point out that the surface has a different density and structure as compared to the interior of the cluster.[4] Furthermore, the surface can be influenced (distorted) by the presence of adsorbed atoms or impurities. An extensive NMR research demonstrated the presence of silanols at the surface.[15] The combined effect can lead to the observed common broadening of the ESR spectra for the as-grown state sample measured immediate upon vuv irradiation. The observed dependence on observational temperature of the overall linewidth can be explained by a temperature dependent surface strain adaptation. The thermal expansion coefficient α_{SiO2} of SiO_2, although overall extremely low, does exhibit a clear temperature dependence, i.e., a monotonic increase, the largest relative variation (a factor $\geqslant 2000$) occurring in the range[48] 6–75 K. Measuring at a higher temperature (77 K) can lead to some relaxation of the surface, thus decreasing the linewidth. A second possible explanation can be found with the adsorbed atoms. As the temperature increases the atoms can start tumbling leading to motional narrowing.[47] As will be demonstrated later, tumbling methyl radicals are indeed observed at these silica nanoparticles.

The effect of the postmanufacture heating on the E' system may also be understood within the above outlined picture. In a first view, the results may be explained by posing that with heating at increasingly higher temperatures in the range $T_{an} \geqslant 850$ °C, the surface E' system is gradually eliminated, through irreversible structural network adaptation or chemical interaction with impurities leading to firm bonding. The former may appear less obvious, while the latter need interference of impurities other than hydrogen. However, in a second more likely view, the surface E' system might just plainly be irreversibly eliminated by heating-dependent reduction of the effective sample surface area through particle sintering. Such sintering is known to start from about 800 °C onward, as recently reevidenced by Uchino *et al.*[11] exposing a decrease in specific surface area with T_{an}, well mimicking (with respect to the pertinent T_{an} range) the E'_γ g_c vs T_{an} dependence currently measured immediately upon vuv activation. While we cannot discriminate between the two interpretations, the latter, given the physical facts, must at least account for part of the E' observations.

All in all, as a main result, the current E' data reveal structural aspects of the nm-sized fumed silica particles different from bulk glassy SiO_2. For one, g matrix alterations are observed, assigned to enhanced amorphous state disorder and strain: Structural variations affect the spatial distribution of the unpaired electron orbital, which in turn, through the spin-orbit coupling, reflects back into the observed g factor. It is interesting to note that in recent work,[49] small relative variations in g matrix elements (principal g values) observed in dry silica as a function of increasing ^{60}Co γ-irradiation (10^{-1}–10^4 kGy) have also been attributed to structural modifications reflecting back in the unpaired electron orbital, thus resulting in g shifts through the spin-orbit coupling.

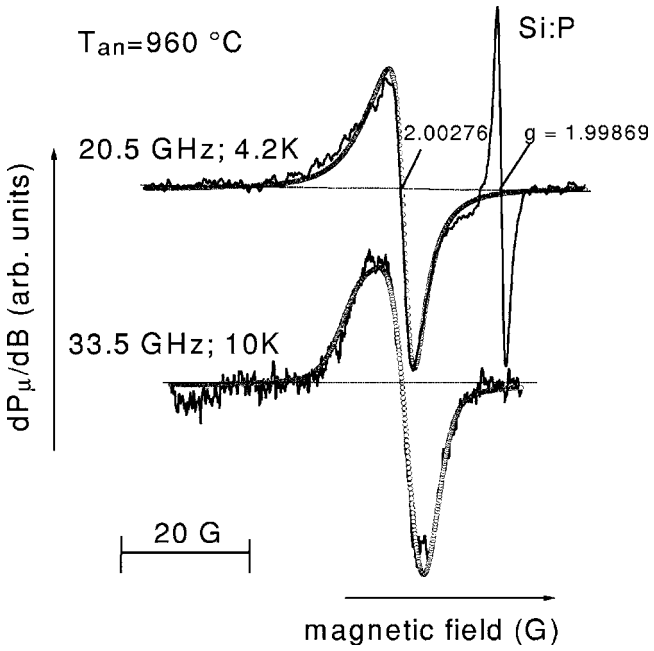

FIG. 4. Powder pattern K-band ($P_\mu \sim 0.3$ nW; $B_m \sim 0.5$ G) and Q-band ($P_\mu \sim 40$ nW; $B_m \sim 0.3$ G) ESR spectra of the observed signal in silica nanoparticles annealed at 960 °C. The symbols represent spectra simulations (see text for parameters).

In a more direct structural picture, it is known that for tetragonally arranged defects, such as the $Si_3 \equiv Si\cdot$ defect (P_b center) at the Si/SiO_2 interface, shifts in, e.g., $g_\parallel$ away from the average value may be directly related to variations in the unpaired bond angle θ (angle between the unpaired sp_3-like orbital direction and a Si-Si back bond). An increase in θ results in a shift in zero crossing g value towards higher values.[50] Shifts in g can thus be directly translated into a more planar or pyramidal defect configuration,[44,20] which may provide useful information, also in the case of the E' center, e.g., in terms of local stress. However, no such clear relationship appears as yet established for the E' center. This will concern a next step in research, implying experimental refinement as well as, perhaps more crucially, substantial theoretical effort.

B. A newly isolated ESR signal

Upon postformation heating an unidentified signal (termed LU2) newly appears in maximum densities $(6.0 \pm 0.6) \times 10^{15}$ g^{-1} ($\sim 2.5 \times 10^{-3}$ defect/particle), without additional vuv excitation, unlike as required for the detection of the E' center. At K band it appears as a single asymmetric signal of $g_c = 2.00276 \pm 0.00005$ and peak-to-peak width $\Delta B_{pp} = 4 \pm 0.2$ G. Figure 4 shows K and Q-band ESR spectra

observed at low T, after annealing the sample at T_{an} =960 °C. The signals exhibit powder pattern properties, and both could be readily consistently simulated (symbols in Fig. 4) by one effective spin $S=\frac{1}{2}$ center, of closely axial symmetry, with one set of g matrix principal values given as $g_{\|}$ =2.0041 and $g_{\perp}=2.0027$; Only the microwave frequency f has been changed and the Lorentzian broadening function has been increased with f. Other observations include: In the range 850–1115 °C, the signal intensity is found to be maximal for $T_{an}\sim 960$ °C; Subjecting the sample to vuv irradiation decreases the intensity of the center.

It is realized, however, that the attained signal-to-noise ratio is limited. So, conforming to scientific rigor, full allowance should be made for other interpretations. For one, rather than adhering to the powder pattern (PP) of one type of defect, e.g., the overlap of two separate signals of different g values, which structure would also broaden with increasing microwave frequency. Through computer simulations, this route has been carefully analyzed. However, despite fitting over a broad range of parameter values ($g, \Delta B_{pp}$, line shape, relative intensity), we failed to realize a match as satisfactory as readily obtained by the single powder pattern interpretation, the main delimiting obstacle appearing to be the observed overall signal symmetry, e.g., the signal measured at Q band at 150 K constitutes a well expressed "two peak" powder pattern. This is why the PP interpretation is favored. Of course, it cannot be excluded that with still increasing the number of independent signals (3 or more), thus concomitantly unrealistically augmenting the number of independent parameters (4 per signal), a satisfactory consistent fit might ultimately be realized—but, obviously, at the cost of scientific credibility.

Without doubt, the first key question concerns the origin of this signal. As is well known from previous studies on atomic identification of point defects, almost exclusively based on ESR analysis, conclusive determination of the nature of the originating defect necessarily requires information on the hf interaction. Identification of the defect is considered much relevant as its appearance may be closely tied to a specific characteristic of the fumed silica network, possibly different from the bulk glassy SiO_2 state. Several attempts were made to resolve associated hf structure from the background, yet so far without success, which makes that the discussion of the center's origin remains largely speculative (*vide infra*).

C. OHC type centers

In Fig. 5, we show overall K and Q-band spectra measured over an extended field range in the liquid nitrogen temperature range. They correspond to the totality of observed ESR signals. A most eye-catching part in these ESR spectra, measured on the as-grown sample immediate upon vuv irradiation, without doubt concerns the left part of the spectra, which exhibits broad resonances. The position and shape of the broad ESR signal(s) points in the direction of the oxygen-associated hole centers (OHC's).[51] The ESR signal was investigated with great care in order to assess more detailed information about the specific ESR features. The

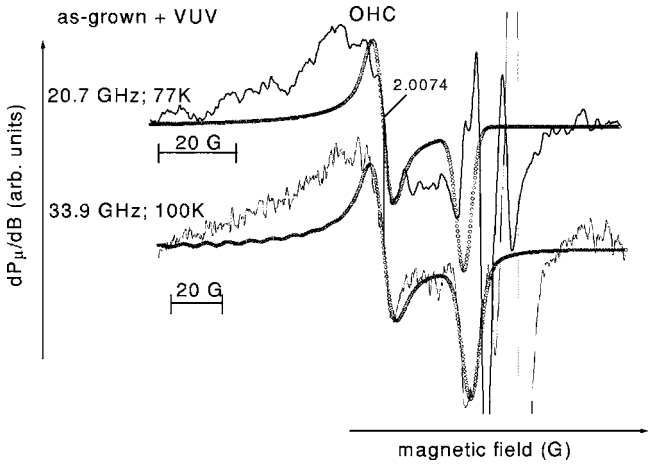

FIG. 5. Overall K-band ($P_\mu\sim 8$ μW; $B_m\sim 0.6$ G) and Q-band ($P_\mu\sim 0.17$ mW; $B_m=1$ G) powder pattern ESR spectra of the as-grown sample after vuv irradiation. Extreme ESR measurement parameters are used to enhance the broad signals in the g range 2.02–2.0015 and to (partially) saturate the other signals (E'-like center, methyl radical) present. The broad resonances centered at $g\sim 2.0074$ are ascribed to OHC centers. The symbols represent peroxy radical spectra simulations; the principal g values used for both spectra simulations are $g_1=2.0020$, $g_2=2.0078$, and $g_3=2.0670$.

spectra were monitored as a function of observational temperature, revealing some striking changes to occur. It became clear that the broad ESR line is the resultant of at least two resonant responses.

One of them, centered at $g_c=2.0074\pm 0.0005$, exhibits powder pattern properties, and could be readily well simulated (symbols in Fig. 5) in the temperature range ~77–100 K—consistently for K and Q-band observations—using a simple spin Hamiltonian of effective spin=$\frac{1}{2}$, with one set of g matrix principal values given as $g_1=2.0020$, $g_2=2.0078$, and $g_3=2.0670$. The latter g_3 is taken from Ref. 39, and in fact is kind of immaterial here, as the corresponding resonance peak in the powder pattern could not be resolved. Interestingly, these ESR parameters are very similar to those pertaining to the well-known peroxy radical (POR) ($O_3\equiv$Si-O-O•).[39] To get more conclusive evidence several attempts were made to resolve the powder pattern peak corresponding with the g_3 component. However, these attempts failed and the signal remained beyond ESR detection, likely due to the low signal intensity and line broadening. Inferred POR densities from simulations were up to $(3.1\pm 0.3)\times 10^{15}$ g^{-1} or about 1×10^{-3} defects/nanoparticle. This would indicate that fumed silica is somewhat *oxygen rich*, which would be consistent with the low density of E' centers (O vacancies) encountered.

The other part of the broad resonance line could not be assigned conclusively. There is a possibility that this line is also related to some (other) type of OHC's, possibly the nonbridging oxygen hole centers (NBOHC) (characterized by[39] $g_1=1.9999$, $g_2=2.0095$, and $g_3=2.078$). But this is more of a suggestion. However, even in lack of full identification, we still can provide, as a useful number, an estimate of the upper limit of the density of all OHC's possibly present from the added intensities of all pertinent signals. This leads to a

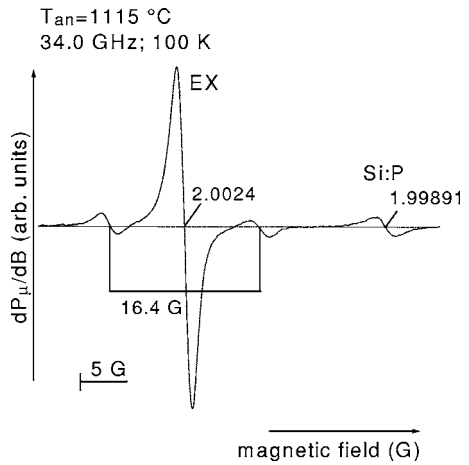

FIG. 6. Q-band ESR spectrum ($P_\mu \sim 0.3$ μW; $B_m=1$ G) of the EX center measured in the samples subjected to postmanufacture baking at $T_{an}=1115$ °C.

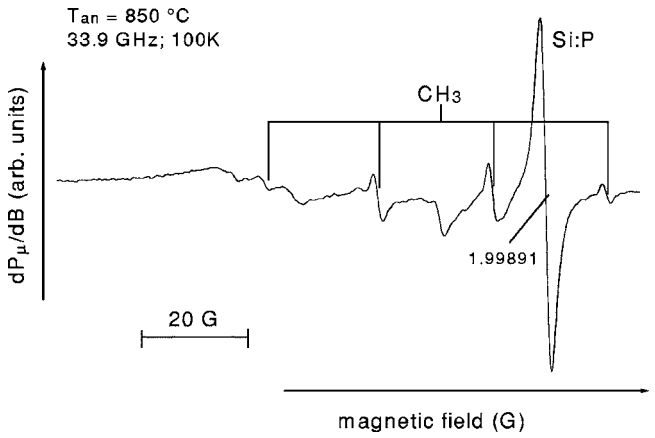

FIG. 7. Q-band ESR spectrum ($P_\mu \sim 0.165$ mW; $B_m=1$ G) of the CH_3 radical observed for the nanoparticles subjected to postmanufacture baking at $T_{an}=850$ °C.

maximum number of OHC defects possibly present of ~0.07 defects/particle. The broad resonance lines, and therefore the OHC's, decrease drastically when subjecting samples to additional heat treatment.

D. EX center

With increasing T_{an}, another signal appears in increasing intensity. The originating defect is conclusively identified as EX, a SiO_2-specific center.[52] In one view, it is pictured as a hole delocalized over 4 nonbridging oxygens grouped around a Si vacancy. The signal is observed from $T_{an} \geqslant 960$ °C on and is most intense [density up to $(4.9\pm0.5)\times10^{15}$ g^{-1}] after annealing at $T_{an}\sim1115$ °C; the intensity generally drops upon vuv irradiation (cf. Table I). A characteristic spectrum is shown in Fig. 6. The measured ESR parameters ($g=2.0024$, hf splitting $A_{hf}=16.4$ G) are characteristic for the well known EX center. The EX center was first reported previously in a systematic study of standard Si/SiO_2 structures with thin ($\leqslant$13 nm) thermally grown SiO_2 films, where the originating defect was found to pertain to the outer (~4 nm) SiO_2 layers. It has since been reported in various works.

E. The methyl radical

A characteristic ESR spectrum (Fig. 7) consisting of 4 hyperfine lines with intensity ratio 1:3:3:1 is observed in the as-grown sample and in the samples annealed up to 1005 °C, measured immediate upon vuv irradiation. This specific intensity ratio is readily explained as originating from a spin system consisting of an unpaired electron $\left(S=\frac{1}{2}\right)$ interacting with three equivalent spin-$\frac{1}{2}$ nuclei. Since the sample is of very high purity the most likely candidates for the nuclei are protons. The measured ESR parameters (average g value $g_{av}=2.0026\pm0.0005$; $A_{hf}=23\pm0.5$ G) are indeed very similar to those observed for the methyl radical.[53] The methyl radical has previously been reported to be present in irradiated amorphous SiO_2,[54] on silica gel surface,[55] and in some irradiated high purity synthetic silica.[56] It leaves no doubt that the observed ESR spectrum originates from the CH_3 radicals.

The total intensity of the spectra was inferred by double numerical integration of the hf component on the outer high field side of the spectrum (the best resolved hf component here, the others being perturbed by signal overlap) and multiplying this intensity by 8. The density of the methyl radicals is the highest, i.e., $(0.047\pm0.005)\times10^{15}$ g^{-1}, for the sample annealed at $T_{an}=850$ °C subjected to vuv. This sample was used for further analysis.

As the measurements were carried out carefully with reduced modulation amplitude to avoid overmodulation, it became clear that the linewidths depend on the nuclear spin quantum number (M_I). This observation can be interpreted as the result of the tumbling of a spin system with anisotropies in the hyperfine interaction and g matrix, which provides a relaxation mechanism dependent on M_I.[57] When ESR measurements where carried out at a temperature below 85 K, the ESR lines broadened beyond ESR detection. This result suggests that the radicals "freeze" at low temperatures, substantiating that they are indeed tumbling when measured at a sample temperature of about 100 K.

The tumbling frequency can easily be calculated (see Ref. 55 and the references therein). The linewidth in terms of inverse transverse relaxation time can be expressed as a sum of a secular, pseudosecular, and nonsecular part

$$(T_2)^{-1} = (T_2)^{-1}_{\text{sec}} + (T_2)^{-1}_{\text{pseudosec}} + (T_2)^{-1}_{\text{nonsec}}. \quad (1)$$

Since the nonsecular contribution to the linewidth is completely negligible and the pseudo-secular contribution is negligible to a fair approximation (~10%), the expression for the linewidth can be reduced to

$$(T_2)^{-1} = a_0 + a_1 M_I + a_2 M_I^2. \quad (2)$$

The constants can be evaluated as

$$a_0 = \frac{4}{45}(\Delta\gamma B)^2 \tau_c + K,$$

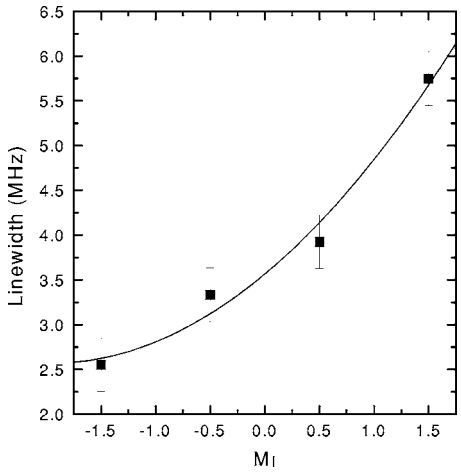

FIG. 8. Linewidths of the four hyperfine components of the methyl radical spectrum as a function of corresponding nuclear magnetic quantum number. The dots are the experimental points; the solid line represents the fitted curve based on Eq. (2) (see text).

$$a_1 = \frac{4}{15} b \Delta\gamma B \tau_c,$$

$$a_2 = \frac{1}{5} b^2 \tau_c, \tag{3}$$

where τ_c is the correlation time, b the hf anisotropy, B the magnetic field, $\Delta\gamma$ the g matrix anisotropy, and K contains other unspecified contributions to the linewidth that are independent of M_I.

The linewidths were measured and least squares fitted using Eq. (2). It should be noted that the determination of the exact linewidths was somewhat hampered because of signal overlap. The measured linewidths and calculated fit are shown in Fig. 8. The inferred constants are $a_0 = 3.656$ MHz, $a_1 = 1.017$ MHz, and $a_2 = 0.259$ MHz. If using the value $b = 4.5$ MHz, obtained by Heller[58] for the CH_3 group in the radical $CH_3C(COOH)_2$, as an estimate for the hf anisotropy of the methyl radical, the correlation time and thus the tumbling frequency can be calculated. In this way we find $\tau_c = 6.39 \times 10^{-8}$ s, giving 1.56×10^7 s^{-1} for the tumbling frequency. The latter value is in between the value inferred for the methyl radical trapped in irradiated high purity fused silica[56] (1.1×10^7 s^{-1}) and the value obtained for the radical adsorbed on the silica gel surface[55] (2×10^7 s^{-1}). It seems that in fumed silica the radical's rotation is slightly more hindered compared to the methyl radicals adsorbed on a silica gel surface, but less hindered by the silica network as compared to the methyl radicals present in irradiated fused silica.

It should be noted that in fumed silica the methyl radicals are possibly less stable than the ones observed in irradiated fused silica. In the latter case Friebele *et al.* still measured the same defect densities after keeping the sample for two years in room ambient.[56] In fumed silica, however, the defect densities decreased beyond ESR detection already several days after irradiation.

The appearance of CH_3 radicals is a general indicator of carbon and H contamination. This may not come as a surprise with respect to hydrogen, the abundance of which has been amply demonstrated previously by numerous techniques.[9,15] However, despite no carbon should be present during the fabrication of fumed silica, the nanoparticles are clearly C contaminated since the methyl radicals are observed in the as-grown state. Apart from possible C impurification during manufacturing, another possibility is C contamination arising from surface adsorbance of C-containing species (e.g., CO, CO_2) from room ambient. Given the particles large area aspect, the latter may appear most likely.

For completeness, we add that in the synthetic fused silica study using ^{60}Co γ irradiation,[56] the CH_3 radical formation is ascribed to radiodissociation of CH_4 or CO molecules trapped in the silica network during silica formation. Also, soaking silica in high-pressure methane failed to produce methyl radicals after subsequent irradiation.

IV. DISCUSSION

One particular point of interest is the atomic structure of the additionally observed unknown signal LU2. Addressing this may reveal important information on the fumed silica's network structure. As no associated hf structure could be resolved from the background the center's origin remains elusive. Purely based on g_c, one possible candidate could be the S center ($g_c \sim 2.0027$), tentatively assigned[24,59] to the E'-like centers $Si_nO_{3-n}{\equiv}Si\cdot$ (n=1,2), likely $SiO_2{\equiv}Si\cdot$. That center was also revealed after high-T annealing in vacuum, prominently so in thermally grown SiO_2 layers on Si. However, at first sight, general linewidth and g matrix asymmetry considerations would disfavor this assignment.

In looking further for other models, given the measured zero crossing g value $g_c = 2.00276$, we may also consider the possibility that the signal originates from C-related defects. Indeed, many signals observed around that g value (see, e.g., Ref. 60) have been attributed to (identified as) C-related defects, e.g., as encountered in carbonaceous materials such as mechanically damaged[61] C powder ($\Delta B_{pp} \sim 5.5$ G; $g = 2.0027 \pm 0.0002$) and a-SiC films ($\Delta B_{pp} \sim 6$ G; $g = 2.003 \pm 0.001$),[62] and as contaminants on ion-implanted glass[63] and various heat-treated surfaces,[64] the latter, for quartz and glass, characterized by a width ΔB_{pp}(X-band) ~ 1 G and $g = 2.0028$. A singlet characterized by an approximately Lorentzian shape, $\Delta B_{pp}(X\text{-band}; 300\ \text{K}) \sim 1-3$ G and $g = 2.0026 \pm 0.0002$ was reported in virtually all ion-implanted glasses[63] and ascribed to surface C contamination. Along the case of heat-treated surfaces, the observed LU2 signal could have resulted from the annealing in vacuum. However, counter to this interpretation would appear the currently applied high-T_{an} values and the nondisappearance of the ESR signal when exposed to air (room ambient).[64] But it is well realized that for unequal circumstances (e.g., material, shape, treatment) signals may appear different, and a possible relationship of LU2 to carbon is not ruled out; However, it cannot be substantiated any further either. Thus, conclusive identification of this (new) defect remains still open.

The overall ESR spectra measured on the as-grown sample immediately upon vuv irradiation is dominated by (a)

signal(s) that can possibly be assigned to OHC type defects. An estimate was made of the upper limit of all OHC's possibly present in the as-grown sample upon vuv activation, where the density was determined for different vuv irradiation times in order to ensure that most, if not all, of the centers present are indeed ESR activated (attaining density saturation level). The maximum density determined is ~0.07 defects/particle. As aforementioned, Altman *et al.* suggested that these OHC centers would be present in such concentrations that they may cause narrowing of the optical energy gap through strong Coulomb disorder.[14] The current observations, however, disfavor this suggestion, at least in a statistically uniform picture, since for these defects to cause changes in the bandgap there should be at least more than one defect present in each nanoparticle. By contrast, our data indicate that, as an upper limit, only one in about every 14 particles may house such defect. Of course, defect bunching cannot be excluded, i.e., a small minority of particles could contain several to many OHC's per particle, the remainder and major portion of the SiO_2 particles then being OHC free. We would have two particle subsystems in terms of OHC content. However, this may appear unfeasible.

Another point of discussion concerns Glinka *et al.*'s suggestion that the NBOHC's dominate the PL spectrum when the sample is pretreated at $T_{an}=900\ ^\circ C$.[12] The broad ESR resonance line, which can possibly be assigned to some type of OHC's, on the contrary, decreases drastically upon additional heat treatment. It should be mentioned, however, that the postmanufacture heat treatments applied by Glinka *et al.* (2 h in air) differ from those applied in this research (~1 h in vacuum), which, given the nano dimensions of the particles, may be linked to the difference in result attained. This requires further investigation.

V. SUMMARY AND CONCLUSIONS

A systematic ESR study in conjunction with postmanufacture irradiation and/or annealing in the range 850–1115 °C of fumed silica nanoparticles, reveals for the first time the presence of ESR-active point defects. Their generation and properties have been studied systematically by ESR as a function of T_{an} and vuv treatment. Several point defects inherent to the SiO_2 network are revealed, including E'_γ, the O^-_2 ion, and the EX center. The methyl radical is also found to be present. Additionally, an as yet unidentified defect is newly observed. Besides the identified ESR signals, still others are observed who could not be spectroscopically isolated or identified. The presence of these defects and their ESR properties can provide important information on the structural and chemical nature of the fumed silica nanoparticles. Some specific results include the following.

(1) The methyl radical is observed in the as-grown state and after postmanufacture baking in the range 850–1005 °C, immediately upon vuv irradiation. These $\cdot CH_3$ centers are a familiar indicator of trace carbon and hydrogen contamination. At $T\sim 100$ K, it has been inferred that the radicals tumble at a frequency of $1.56\times 10^7\ s^{-1}$. Yet, they appear unstable as their ESR signal intensity decreases beyond ESR detection several days after the vuv activation.

(2) Evidence has been found for the presence of nonbridging oxygen-associated hole centers in the as-grown samples after vuv irradiation. One OHC type occurring appears to be the peroxy radical ($O_3{\equiv}Si\text{-}O\text{-}O\cdot$), which would indicate that fumed silica is somewhat oxygen rich.

(3) An as yet unidentified defect, which may be linked to specific network aspects, is observed in the as-grown samples annealed at $T_{an}=850-960\ ^\circ C$ even without additional vuv treatment. The spectral properties have been studied in detail, aiming its identification. The ESR properties include $g_c=2.00276\pm 0.00005$, closely axial symmetry, and g matrix principal values $g_\parallel=2.0041$ and $g_\perp=2.0027$. As detection of any associated hf structure has so far failed, the atomic nature of the originating defect remains largely unknown. Yet, based on specific ESR properties it is tentatively ascribed to $O_2Si{\equiv}Si\cdot$, an E'-like center with chemically modified backbond arrangement.

(4) The spectroscopic properties of the E' signal have been studied with particular interest since defect analysis can provide access to the nanoparticle structure on atomic level. Accordingly, changes in the zero crossing g value, line shape, and signal intensity as a function of anneal temperature, observational temperature, and elapsed time period between vuv activation and ESR measurement as the sample was kept in room ambient were carefully monitored.

The combination of all the observations on the E' signal hints at the presence of two different systems of E' centers with superposed ESR signals. It is suggested that the core of the nanoparticles exhibits a bulk a-SiO_2 like structure while the surface region is of a different, more strained nature. There appears a complex strain distribution. The E' centers present in the core regions are very similar to the common E'_γ centers present in bulk a-SiO_2. The E' centers in the surface region, however, exhibit different properties. This can be seen as due to enhanced amorphous state disorder and strain at the surface and in near surface layers. Another important factor is that the surface E' system is possibly more apt to environmental chemical and physical interaction (adsorption) impact. As the postmanufacture temperature increases, sintering takes place decreasing the specific surface area[11] and thereby possibly the number of surface E' centers. The overall maximum E' density is small compared to standard thermal a-SiO_2 grown on Si, indicative of a high quality of the fumed silica particles in terms of occurring O vacancies: Only one E' center is detected in about every 1000 nanoparticles.

The current results bear out the usefulness and potential of ESR spectroscopy in assessing atomic properties of nanoparticles. In combination with other pertinent experimental techniques, consistent deeper insight may be attained.

[1] H. K. Kammler and S. E. Pratsinis, Chem. Eng. Process. **39**, 219 (2000).
[2] S. E. Pratsinis, Prog. Energy Combust. Sci. **24**, 197 (1998).
[3] W. J. Stark and S. E. Pratsinis, Powder Technol. **126**, 103 (2002).
[4] A. Roder, W. Kob, and K. Binder, J. Chem. Phys. **114**, 7602 (2001).
[5] I. V. Schweigert, K. E. J. Lehtinen, M. J. Carrier, and M. R. Zachariah, Phys. Rev. B **65**, 235410 (2002).
[6] A. J. Hurd, D. W. Schaefer, and J. E. Martin, Phys. Rev. A **35**, 2361 (1987).
[7] J. H. Page, W. J. L. Buyers, G. Dolling, P. Gerlach, and J. P. Harrison, Phys. Rev. B **39**, 6180 (1989).
[8] T. Campbell, R. K. Kalia, A. Nakano, F. Shimojo, K. Tsuruta, P. Vashishta, and S. Ogata, Phys. Rev. Lett. **82**, 4018 (1999).
[9] B. C. Bunker, D. M. Haaland, T. A. Michalske, and W. L. Smith, Surf. Sci. **222**, 95 (1989).
[10] H. Saito and T. Hyodo, Mater. Sci. Forum **255–257**, 463 (1997).
[11] T. Uchino, A. Aboshi, S. Kohara, Y. Ohishi, M. Sakashita, and K. Aoki, Phys. Rev. B **69**, 155409 (2004).
[12] Y. D. Glinka, S. H. Lin, and Y. T. Chen, Appl. Phys. Lett. **75**, 778 (1999).
[13] Y. D. Glinka, S. H. Lin, and Y. T. Chen, Phys. Rev. B **66**, 035404 (2002).
[14] I. S. Altman, D. Lee, J. D. Chung, J. Song, and M. Choi, Phys. Rev. B **63**, 161402(R) (2001).
[15] C. C. Liu and G. E. Maciel, J. Am. Chem. Soc. **118**, 5103 (1996).
[16] S. M. Prokes, W. E. Carlos, L. Seals, S. Lewis, and J. L. Gole, Mater. Lett. **54**, 85 (2002).
[17] T. Uchino, A. Sakoh, M. Azuma, M. Takano, M. Takahashi, and T. Yoko, J. Phys.: Condens. Matter **14**, 11111 (2002).
[18] D. L. Griscom and M. Cook, J. Non-Cryst. Solids **182**, 119 (1995).
[19] A. Stesmans, Phys. Rev. B **48**, 2418 (1993).
[20] J. T. Yount, P. M. Lenahan, and P. W. Wyatt, J. Appl. Phys. **77**, 699 (1995).
[21] K. L. Brower, Phys. Rev. B **38**, 9657 (1988).
[22] A. Stesmans and V. V. Afanas'ev, Phys. Rev. B **54**, R11129 (1996).
[23] See, e.g., D. L. Griscom, J. Appl. Phys. **58**, 2524 (1985).
[24] A. Stesmans and V. V. Afanas'ev, Appl. Phys. Lett. **69**, 2056 (1996); A. Stesmans, B. Nouwen, and V. V. Afanas'ev, Phys. Rev. B **66**, 045307 (2002).
[25] A. Pusel, U. Wetterauer, and P. Hess, Phys. Rev. Lett. **81**, 645 (1998).
[26] Sigma-Aldrich Inc., Missouri, USA.
[27] D. L. Griscom, Nucl. Instrum. Methods Phys. Res. B **1**, 481 (1984).
[28] A. Revesz, J. Electrochem. Soc. **126**, 122 (1979).
[29] T. E. Tsai, D. L. Griscom, and E. J. Friebele, Phys. Rev. Lett. **61**, 444 (1988).
[30] H. Hosono, Y. Ikuta, T. Kinoshita, K. Kajihara, and M. Hirano, Phys. Rev. Lett. **87**, 175501 (2001).
[31] D. Donadio and M. Bernasconi, Phys. Rev. B **71**, 073307 (2005).
[32] K. Awazu and H. Kawazoe, J. Appl. Phys. **94**, 6243 (2003).
[33] D. B. Kerwin and F. L. Galeener, Phys. Rev. Lett. **68**, 3208 (1992).
[34] A. A. Bobychev and V. A. Radzig, Kinet. Katal. **32**, 1234 (1990).
[35] A. H. Edwards, J. Non-Cryst. Solids **187**, 232 (1995).
[36] G. Pacchioni and M. Vitiello, Phys. Rev. B **58**, 7745 (1998).
[37] D. L. Griscom, Nucl. Instrum. Methods Phys. Res. B **46**, 12 (1990).
[38] W. L. Warren, E. H. Poindexter, M. Offenberg, and W. Müller-Warmuth, J. Electrochem. Soc. **139**, 872 (1992).
[39] D. L. Griscom, Glass Sci. Technol. (Amsterdam, Neth.) **48**, 151 (1990).
[40] P. G. Tello, V. V. Afanas'ev, and A. Stesmans, Microelectron. Eng. **72**, 81 (2004); A. Stesmans and V. V. Afanas'ev, J. Appl. Phys. **97**, 033510 (2005).
[41] C. L. Marquardt and G. H. Sigel, Jr., IEEE Trans. Nucl. Sci. NS-**22**, 2234 (1975).
[42] R. H. Silsbee, J. Appl. Phys. **32**, 1459 (1961).
[43] G. Hochstrasser and J. F. Antonini, Surf. Sci. **32**, 644 (1972).
[44] M. E. Zvanut, F. J. Feigl, W. B. Fowler, J. K. Rudra, P. J. Caplan, E. M. Poindexter, and J. D. Zook, Appl. Phys. Lett. **54**, 2118 (1989).
[45] B. P. Lemke and D. Haneman, Phys. Rev. B **17**, 1893 (1978).
[46] F. J. Feigl and J. H. Anderson, J. Phys. Chem. Solids **31**, 575 (1969).
[47] M. S. Stoneham, Rev. Mod. Phys. **41**, 82 (1969).
[48] G. K. White, Cryogenics **4**, 2 (1964).
[49] S. Agnello, R. Boscaino, G. Buscarino, M. Cannas, and F. M. Gelardi, Phys. Rev. B **66**, 113201 (2002).
[50] N. Ishii, M. Kumeda, and T. Shimizu, Jpn. J. Appl. Phys. **20**, L673 (1981); Y. Fu and P. A. Fedders, Solid State Commun. **84**, 799 (1992).
[51] M. Stapelbroek, D. L. Griscom, E. J. Friebele, and G. H. Sigel, Jr., J. Non-Cryst. Solids **32**, 313 (1979).
[52] A. Stesmans and F. Scheerlinck, Phys. Rev. B **50**, 5204 (1994); J. Appl. Phys. **75**, 1047 (1994).
[53] See, e.g., F. Gerson and W. Huber, *Electron Spin Resonance Spectroscopy of Organic Radicals* (Wiley, Darmstadt, 2003).
[54] W. R. Austin and R. G. Leisure, J. Appl. Phys. **80**, 6646 (1996).
[55] C. L. Gardner and E. J. Casey, Can. J. Chem. **46**, 207 (1968).
[56] E. J. Friebele, D. L. Griscom, and K. Rau, J. Non-Cryst. Solids **57**, 167 (1983).
[57] H. M. McConnell, J. Chem. Phys. **25**, 709 (1956).
[58] C. Heller, J. Chem. Phys. **36**, 175 (1962).
[59] A. Stirling and A. Pasquarello, Phys. Rev. B **66**, 245201 (2002).
[60] Y. Bounouh, L. Chahed, A. Sadki, M. L. Thèye, C. Cardinaud, M. Zarrabian, J. von Bardeleben, K. Zellama, and J.-L. Fave, Diamond Relat. Mater. **4**, 492 (1995).
[61] G. K. Walters and T. L. Estle, J. Appl. Phys. **32**, 1854 (1961).
[62] M. H. Brodsky and R. S. Title, Phys. Rev. Lett. **23**, 581 (1969).
[63] D. L. Griscom, C. I. Merzbacher, R. A. Weeks, and R. A. Zuhr, J. Non-Cryst. Solids **258**, 34 (1999).
[64] R. C. Henderson, W. J. Polito, and J. Simpson, Appl. Phys. Lett. **16**, 15 (1970).